NOTICE: This is the author's version of a work that was accepted for publication in Soil Dynamics and Earthquake Engineering. Changes resulting from the publishing process, such as peer review, editing, corrections, structural formatting, and other quality control mechanisms may not be reflected in this document. Changes may have been made to this work since it was submitted for publication. A definitive version was subsequently published in Soil Dynamics and Earthquake Engineering 166:107763, 2023. doi.org/10.1016/j.soildyn.2023.107763

Deep vibratory compaction simulated using a high-cycle accumulation model

Patrick Staubach[i)] ; Ivo Kimmig[ii)]; Jan Machaček[iii)] ;
Torsten Wichtmann[iv)] ; Theodoros Triantafyllidis[v)]

April 25, 2023

Abstract: Deep vibratory compaction (DVC) is an effective ground improvement method for granular soils in a loose initial state. An efficient numerical approach to simulate the whole process of DVC considering multiple compaction stages with over 1,000 vibrator cycles per stage is presented. The consideration of such a large number of cycles is made possible by applying an extended high-cycle accumulation (HCA) model. The approach allows to determine the optimal duration of vibration per compaction stage and the spacing of the stages of the DVC process. It is shown that a short vibration time per compaction stage with a small vertical distance between stages is favourable from an economical point of view.

Keywords: Ground improvement; deep vibratory compaction; densification; HCA model

1 Introduction

In case of loosely bedded non-cohesive soils various ground improvement methods offer economical and ecological solutions to obtain save and reliable foundations of buildings and structures without the use of costly pile foundations or diaphragm walls. Especially for the densification of granular soil with less than 15 % fines content of the grain size distribution in large-scale projects, e.g. land reclamation areas and deposits of open pit mines, deep vibratory compaction (DVC) is used in construction practice [23, 35, 4, 17]. Most important part of DVC treatments is the electrically or hydraulically driven deep vibrator with diameters of about 0.3 m to 0.5 m which reaches down to depths of 50 m and below. Efficient compaction is achieved by application of predominantly horizontally oscillating movements of the deep vibrator.

DVC treatments are subdivided in three phases: Insertion phase, withdrawal phase and surface compaction [13]. During insertion phase the oscillating vibrator (frequency $f \approx 25$ to 40 Hz) with connected extension tubes is brought into the subsoil under its own weight. The insertion process is supported by water flushing with water jets at the bottom and top end of the vibrator developing a small annulus around the vibrator where smaller grain particles are flushed towards the ground surface. As soon as the final depth is reached, the flushing is usually stopped. While vibrating, the vibrator is held for about 30 s to 90 s in a certain depth and is pulled up afterwards in 0.3 m to

[i)]Chair of Geotechnics, Bauhaus Universität Weimar, Germany/Chair of Soil Mechanics, Foundation Engineering and Environmental Geotechnics, Ruhr Universität Bochum, Germany. Email: patrick.staubach@uni-weimar.de, Corresponding author.

[ii)]Keller Grundbau GmbH, Germany

[iii)]Institute of Geotechnics, Technische Universität Darmstadt, Germany/Chair of Soil Mechanics, Foundation Engineering and Environmental Geotechnics, Ruhr-Universität Bochum, Germany

[iv)]Chair of Soil Mechanics, Foundation Engineering and Environmental Geotechnics, Ruhr-Universität Bochum, Germany

[v)]Chair of Soil Mechanics, Foundation Engineering and Environmental Geotechnics, Ruhr-Universität Bochum, Germany

1 m steps. This step by step procedure is continued until the vibrator reaches the ground surface. Usually vibrator frequencies between 20 Hz to 30 Hz are used in the withdrawal phase. As a result an improved, compacted soil volume of limited radial extent and significantly lower void ratio e respectively higher relative density D_r is obtained. Due to relatively low mean effective stresses near the ground surface the induced vibrations of the deep vibrator cause dilatant behavior of the soil which leads to an increase of void ratio in the upper 1-2 m of the ground. Thus surface compaction and preparation of a planum level is necessary after completion of DVC prior to the creating of a foundation.

Three areas in the soil around the deep vibrator can be identified. The area referred to as the "fluidised zone" is in direct contact with the vibrator and undergoes large deformations [52]. With increasing distance to the vibrator, smaller deformations are generated in the surrounding soil. In this area, the loading with a high number of loading cycles causes an accumulation of deformations. This "accumulation zone" is ultimately the zone where the actual compaction takes place and the existing pore space is increasingly reduced. It is also the zone for which the present work aims to develop a numerical model for. For larger distances almost no permanent plastic deformations occur and only elastic waves propagate further. This distance represents the transition to the so-called "elastic zone" and thus describes the transition to the existing, uncompacted soil.

In most cases the compaction points are arranged within a grid of equilateral triangles with distance x between the compaction points (see Fig. 1). The objective is to guarantee that especially in the vicinity of the neuralgic points (blue dots in Fig. 1), with greatest distance to the vibrator, compaction of the soil reaches required values. Therefore planning and economical realization of large-scale DVC treatments can be seen as an optimization problem with the aim to choose the distance x as large as possible satisfying at the same time the densification criteria.

Up to now the grid design has been chosen based on experience with similar soils throughout the construction practice. Reason for this is beside others that numerical modelling of vibro compaction treatments is a very challenging task:

- In addition to a radially acting force, the movement of the deep vibrator generates shear stresses in the soil, which significantly influence the compaction effect. The movement of the vibrator is schematically shown in top view in Fig. 2. The centre of the vibrator follows approximately a circular movement (the radius of the path of the centre of the vibrator is exaggerated in the illustration). Only a fraction of the soil surrounding the vibrator is pushed laterally by the vibrator, while the soil at the opposite side is unloaded. The compaction is only slightly caused by pressure but is mainly caused by shearing of the surrounding soil [45, 15]. Because of the circular path of movement, modelling the vibrator and the soil axisymmetrically is not expedient and a full 3D model is required. Using an axisymmetric model, both the complex alternating stress path of loading/unloading and the shear stresses in the horizontal plane would not be accounted for.

- Conventional constitutive soil models predict too large accumulation of deformations per cycle at cycle numbers in the range $N > 100$, which is why compaction is usually predicted to be too fast for numbers of cycles experienced during the DVC process ($N > 1000$ for one compaction stage) [45]. Furthermore, the computational effort with an incremental material model is very high for large numbers of cycles. Therefore, special accumulation models are required to describe a compaction process with several hundred or thousand cycles.

- Modelling the vibratory compaction from the vibrator tip to the ground surface as a complete 3D finite element model involves an enormous computational effort and is therefore only suitable to a limited extent for parameter studies. In combination with a rate-dependent material model and especially when dynamic effects are taken into account, this effort increases again significantly.

The numerical approaches presented in the literature so far have only considered a small number of cycles of the vibrator, were restricted to the modelling of one compaction stage only and employed constitutive models unsuitable to predict the soil behaviour under a large number of cycles [27, 14, 3, 8, 24]. The entire process of DVC, i.e. the continuous pulling of the vibrator with multiple compaction phases applying a suitable constitutive model, could not be realistically modelled

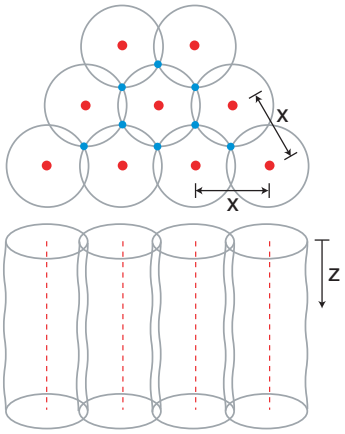

Fig. 1: Schematic compaction grid design using equilateral triangles consisting of red marked vibrator application points. Blue marked points represent neuralgic points with areas of lowest compaction [16].

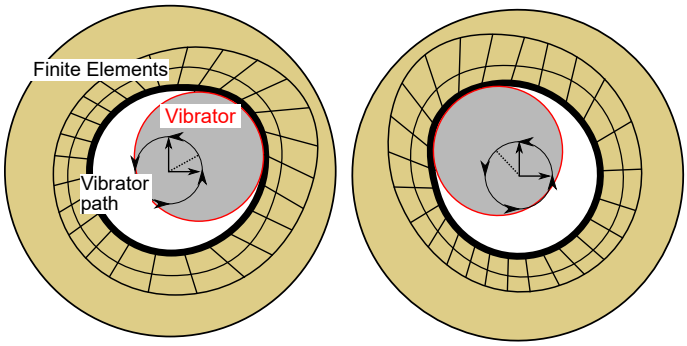

Fig. 2: Schematic illustration of the movement of the vibrator in top view (the radius of the path of the centre of the vibrator is exaggerated for illustration purposes).

up to now. Conventional constitutive models such as the hypoplastic model with intergranular strain extension or the Sanisand model can only realistically capture a limited number of load cycles and predict a nearly linear increase of accumulated strain with increasing number of cycles [47]. In reality, however, the accumulation rate continuously decreases with number of cycles [46]. Special constitutive models such as the high-cycle accumulation (HCA) model by Niemunis et al. [33] are required for a larger number of cycles. This constitutive model was specially developed to calculate the accumulated strain of non-cohesive soils for a large number of loading cycles and has proven a versatile tool for various geomechanical analyses with a large number of cycles (see e.g. [34, 41, 12, 37, 48] for application to monopiles for offshore foundations, [53] for gravity foundations for offshore foundations or [19] for ship locks). Following the general approach presented in [45], the application of the HCA model to the modelling of the DVC process is explained in the next sections.

2 High-cycle accumulation model

In a conventional analysis, every individual cycle is simulated (see Fig. 3a). In contrast, a combined low-cycle and high-cycle calculation strategy (also referred to as implicit-explicit strategy) is used in the HCA model. The procedure is shown in Fig. 3b in a simplified form. The dynamic movement of the deep vibrator with cyclic loading and unloading generates deformations in the soil. Considering an element near the vibrator, the accumulated strain is increasing with time or with the number of loading cycles. Each cycle corresponds to one revolution of the vibrator. For a large number of cycles each individual cycle can hardly be calculated with a conventional (incrementally nonlinear) material model: the result would be a very high calculation effort and the summation of numerical errors due to a large number of iterations. Therefore, a division into a low-cycle and a high-cycle calculation part is proposed. First, a few cycles are simulated with the conventional constitutive model in the low-cycle mode. During the last cycle, the strain path is recorded and the strain amplitude $\varepsilon^{\mathrm{ampl}}$ is determined based on a tensorial strain amplitude A^N [33]. With the strain amplitude as a basis, only the trend of the accumulated strain is then described in the high-cycle mode. During the high-cycle mode, the strain amplitude is a function of the soil stiffness using a so-called adaptive strain amplitude [40], which, contrary to the original formulation [33], takes into account the stiffness changes caused by the cyclic loading.

In analogy to a conventional constitutive model, the HCA model links stress rates with strain rates:

$$\mathring{\boldsymbol{\sigma}} = \mathsf{E} : \left(\dot{\boldsymbol{\varepsilon}} - \dot{\boldsymbol{\varepsilon}}^{\mathrm{acc}} - \dot{\boldsymbol{\varepsilon}}^{\mathrm{pl}}\right). \tag{1}$$

$\mathring{\boldsymbol{\sigma}}$ is the objective (a rigid rotation does not cause any change in stress) stress rate. To obtain an objective stress rate, the Zaremba-Jaumann [54, 11] stress rate is applied in this work, which is integrated using the Hughes-Winget algorithm [9].

Of major importance is the accumulation rate $\dot{\boldsymbol{\varepsilon}}^{\mathrm{acc}} = \boldsymbol{m} \cdot \dot{\varepsilon}^{\mathrm{acc}}$, which is calculated using the flow direction $\boldsymbol{m}$ of the Modified Cam-Clay (MMC) model and the accumulation intensity $\dot{\varepsilon}^{\mathrm{acc}}$. The flow direction of cohesionless soils subjected to

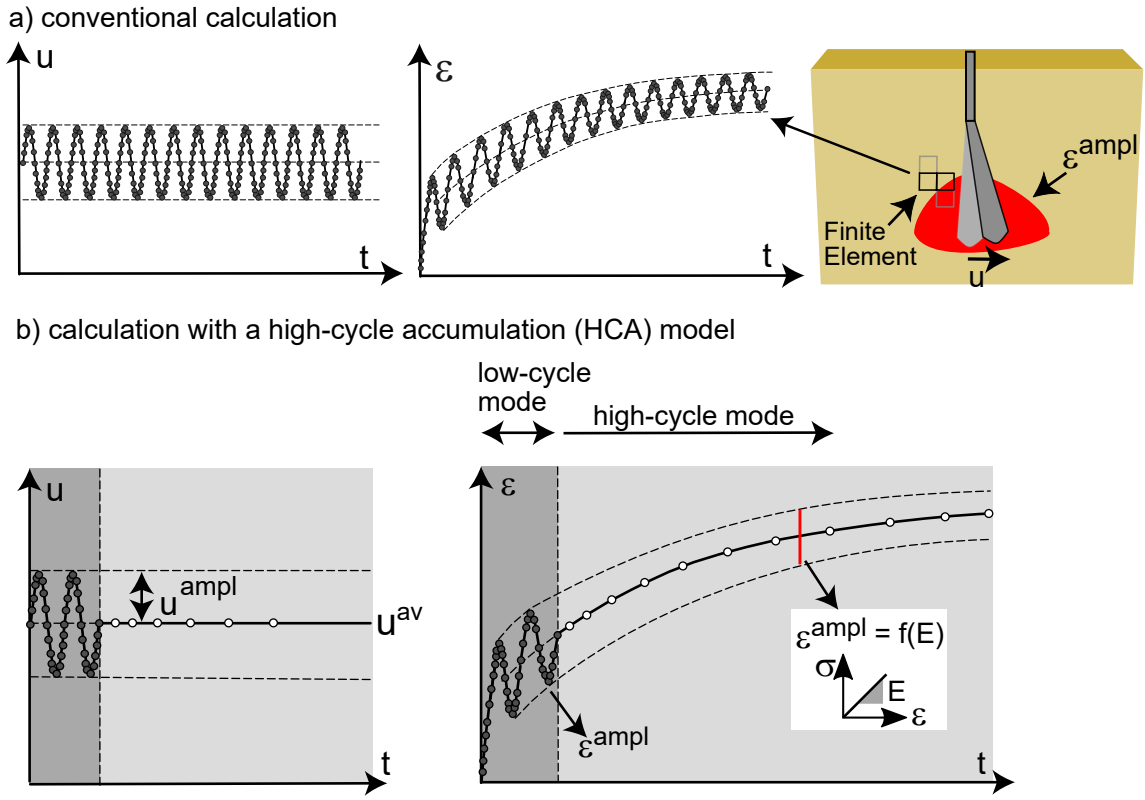

Fig. 3: Calculation strategy in conventional analyses and in simulations using the HCA model (modified from [47]). For simulations with the HCA model the strain amplitude $\varepsilon^{\mathrm{ampl}}$ is determined from the second load cycle calculated with a conventional constitutive model. Only the trend of strain accumulation is predicted in the high-cycle mode. During the high-cycle mode, the strain amplitude is a function of the soil stiffness using a so-called adaptive strain amplitude [40].

cyclic loading has been investigated in an extensive laboratory testing program [46, 49]. It was found that the average stress ratio is the decisive variable influencing the direction of accumulation. Effects resulting from changes in the density and the structure of the soil have only a minor influence. Therefore, the flow direction of the MCC model, which only considers the influence of the average stress ratio, was found to be sufficient. Since the average stress ratio changes during the cyclic loading in general (see Eq. (1)), the flow direction is influenced by the number of load cycles.

Within the HCA model the accumulation intensity is determined by multiplication of five functions, which take into account the influence of the strain amplitude, the mean effective stress, the stress ratio and the void ratio. In addition, the influence of cyclic preloading is considered using the preloading variable g^A, which weights the number of applied cycles N by the strain amplitude $\varepsilon^{\mathrm{ampl}}$ of these cycles. Details on the definition of $\dot{\varepsilon}^{\mathrm{acc}}$ can be found in [31, 47]. $\dot{\boldsymbol{\varepsilon}}^{\mathrm{pl}}$ is only active in case the stress reaches the Matsuoka-Nakai failure locus.

Equation (1) considers rates of stress and strain with respect to number of cycles and not with respect to time. In transient analyses, i.e. analyses performed in physical time, the integration of Eq. (1) is performed using $\Delta N = \Delta t / t_{\mathrm{cycle}}$, where Δt is the time increment applied by the FE program and t_{cycle} is the duration of a single cycle. This is relevant in the present work since consolidation is accounted for. For the application of the HCA model to the simulation of a dynamic boundary value problem (BVP), it is assumed that the accumulation of permanent strain does not lead to a change of the average acceleration. Then it is sufficient to calculate the strain amplitude in a dynamic analysis and perform the high-cycle calculation neglecting inertia forces, since they are incorporated in the strain amplitude. This assumption depends on how large the rate of stress calculated by Eq. (1) is. The larger the stress rate, the less justified is the assumption of the average acceleration being constant because the momentum balance then requires acceleration to ensure equilibrium. The accumulation of stresses depends on

C_{ampl}	C_e	C_p	C_Y	C_{N1} $[10^{-5}]$	C_{N2}	C_{N3}
2.25	0.50	0.41	2.59	5.91	0.15	0

Table 1: Parameters of the HCA model for "Karlsruhe Sand"

the BVP. For instance, in a drained cyclic triaxial test, the stress rate is zero and an unconstrained accumulation of strain occurs. Therefore, independent of frequency of loading, the average inertia effects will be constant (i.e. zero in a steady state) and only the inertia forces of an individual cycle matter. This allows to neglect the inertia terms in the HCA analysis, which only works in terms of average values. Typically, the average stress rate per cycle is also low for more complicated BVPs, such as deep vibratory compaction, justifying the application of the HCA model.

A total of seven material model parameters have to be calibrated using results of drained cyclic triaxial tests. Therefore, drained triaxial and hollow cylinder tests with a large number of cycles and comparable large strain amplitudes ($\varepsilon^{\text{ampl}} > 5 \cdot 10^{-3}$) have been performed, which are documented in [16]. Typically, the strain amplitude during the DVC process is lower than $5 \cdot 10^{-3}$ in a distance of approximately 1 m from the vibrator. This holds even for large displacement amplitudes of the vibrator of ≈ 1 cm [45]. Considering that the presented approach does not aim to fully describe the mechanisms in the "fluidised zone" around the vibrator, it is judged appropriated to use parameters in this zone which are not specifically calibrated for $\varepsilon^{\text{ampl}} \gg 5 \cdot 10^{-3}$. A medium coarse sand ("Karlsruhe Sand") has been considered in the drained triaxial and hollow cylinder test. The parameters obtained from the calibration of the HCA model using these laboratory results are given in Table 1 and are used for the simulations presented in Section 4.

It is worth mentioning that, based on approximately 150 drained cyclic triaxial tests, a simplified calibration procedure has been proposed in [50]. All parameters given in Table 1 can be estimated based on the mean grain size d_{50}, the uniformity coefficient C_u and minimum void ratio $e_{\min}$. However, it is recommended to conduct at least one drained high-cyclic triaxial test in order to calibrate the parameters considering the cyclic preloading C_{N1}, C_{N2} and C_{N3}, used to describe the development of accumulated strain with increasing number of cycles. For the simulation of the DVC process, where only a rather rough estimation of the achieved densification pattern is required, the determination of all parameters based on the above mentioned basic soil properties is probably sufficient.

As is indicated in Fig. 3, the strain amplitude is not constant during the high-cycle phase but is continuously updated using a so-called adaptive strain amplitude [40]. Changes in the soil stiffness resulting from the change in the soil state can therefore be accounted for. For this purpose the following relation between the tensorial strain amplitude and the soil stiffness is employed:

$$\mathsf{A}^N = \mathsf{A}^0 \frac{\|\mathsf{E}^0\|}{\|\mathsf{E}^N\|}. \tag{2}$$

Therein, A^N is the tensorial amplitude and E^N the soil stiffness at N cycles. A^0 and E^0 are the corresponding reference values obtained from the second load cycle in Fig. 3. Once updated, the scalar strain amplitude $\varepsilon^{\text{ampl}}$ is obtained following the procedures described in [33]. The soil stiffness is obtained from the constitutive model used to calculate the strain amplitude, which is the hypoplastic model with intergranular strain in this work. The stiffness inserted in Eq. (2) is calculated by numerical differentiation giving a tangent stiffness. Details on this procedure can be found in [40].

A spatial smoothing of the field of strain amplitude is necessary once updated. The spatially smoothed value $\bar{\varepsilon}^{\text{ampl},N}$ is calculated using

$$\bar{\varepsilon}^{\text{ampl},N}(\boldsymbol{x}_i) = \int w(\boldsymbol{x}_i, \boldsymbol{x}_j) \varepsilon^{\text{ampl},N}(\boldsymbol{x}_j) \, \mathrm{dV} \,. \tag{3}$$

Therein, $\boldsymbol{x}_i$ denotes the coordinate of the integration point at which the strain amplitude is smoothed and $\boldsymbol{x}_j$ are the coordinates of all adjacent points considered for the smoothing. $w(\boldsymbol{x}_i, \boldsymbol{x}_j)$ is a weight function, which is chosen to be the Gaussian function ("bell curve"). A so-called characteristic length l_c has to be introduced, which influences the distance to other points which are considered for the smoothing. The larger l_c, the more points are considered in the smoothing of the strain amplitude in one point. $l_c = 1$ m is set for all simulations performed in the framework of this paper. More details on the importance of the spatial smoothing can be found in [40].

As is further elaborated on in Section 4, the adaptive strain amplitude definition is a key feature in the simulation of multiple stages of the

DVC process.

3 Calculation of the initial strain amplitude

The first cycles of the vibrator are modelled in a Coupled Eulerian-Lagrangian (CEL) analysis with an explicit time integration scheme considering inertia. Hydro-mechanically coupled analyses are performed, taking into account excess pore water pressures and consolidation processes. In contrast to the simulations reported in [27], the acceleration is considered in the momentum balance of the pore water using the extension of the approach by [6] presented in [39], being of great relevance for the vibro compaction process due to the high accelerations. In addition, cavitation is accounted for, such that the absolute pore water pressure can not drop below the atmospheric pressure. This is done by defining a case for the mass balance of pore water, for details see [38]. The water table is assumed to be identical to the ground surface level.

The movement of the deep vibrator in the soil can only be measured with great effort and depends on a large number of influencing factors [28, 29, 5]. These include among others, the unbalanced mass, the frequency and the arrangement of the vibrator "fins". The results of field tests by Nagy et al. [30] are the basis for the following assumptions. The stated objective of this work is to estimate the compaction based on of a previously calculated field of strain amplitude. Therefore, the motion of the deep vibrator is deliberately modelled in a displacement-controlled manner in order to obtain comparable induced deformations With a force-controlled vibrator motion, the induced deformations are directly dependent on the material behaviour, so that the boundary condition can vary between different conditions. The measurement results of Nagy [28] have shown that the centre axis of the vibrator, starting from a pivot point, describes a geometric figure in the form of a double cone. To reproduce this behaviour, the rigid-body model of the deep vibrator is set in motion in the CEL calculations by cyclically varying the rotational degrees of freedom at the reference point (theoretical pivot point). Figure 4 shows schematically how the deflection of the vibrator is achieved. Here, the angles of twist θ_x about the local x-axis as well as θ_y about the y-axis are controlled simultaneously by given sinusoidal functions. For all simulations $u_x = u_y = 5$ mm is set and the frequency is 25 Hz. Note that the amplitudes are assumed to remain constant throughout the process, which is not necessarily the case in reality because of the densification already experienced with ongoing vibration [28]. The initial depth of the tip of the vibrator is assumed to be 15 m below the ground level. The diameter of the vibrator is 0.4 m and the length of the vibrator h given in Fig. 4 is 3.8 m. The insertion phase of the vibrator into the soil prior to vibration is not modelled.

The hypoplastic model [51] with intergranular strain extension [32] is used for the simulation of the first two cycles of the DVC process. "Karlsruhe Sand" is considered as soil, for which the parameters calibrated in [16] are used. An initially loose state of the soil ($D_{r0} = 0.3$) prior to vibro compaction is assumed. In practice, the initial density is in most cases obtained by means of cone penetration testing (CPT) and application of suitable correlations [18]. In some circumstances (large projects and/or large uncertainties), more sophisticated calibration of the parameters used in the correlation equations might be necessary e.g. by performing CPTs in a calibration chamber. Typically, one would expect that the final density achieved close to the vibrator does not depend too strongly on the initial density (assuming all other parameters remain constant) [25].

The numerical model used for the CEL analysis and the results of these simulations are presented in detail in [16]. They are not discussed in detail here, as they only serve to obtain the field of the initial strain amplitude, which is the input for the simulations with the HCA model presented in the next section. Alternatively, the strain amplitude can also be obtained using the analytical approach presented in [45].

4 Modelling of multi-stage compaction using the HCA model

The finite-element code `numgeo` (Machaček & Staubach, see e.g. [22, 20, 42, 38] and `www.numgeo.de`) is employed for the modelling of multi-stage compaction using the HCA model in a fully Lagrangian analysis. The spatial distributions of the state variables (void ratio, stress and strain amplitude) are imported in the fully Lagrangian model by means of a nearest neighbour search following the procedures described in [7, 39]. Compared to the CEL model described in [16], the Lagrangian model is considerably smaller since quasi-static analysis are performed, for which lower requirements for the distance to the boundaries are to

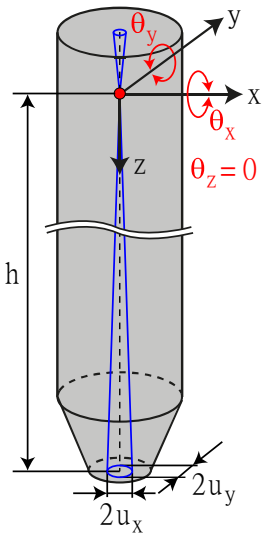

Fig. 4: Schematic representation of the rotational boundary conditions at the reference point (theoretical pivot point) of the deep vibrator

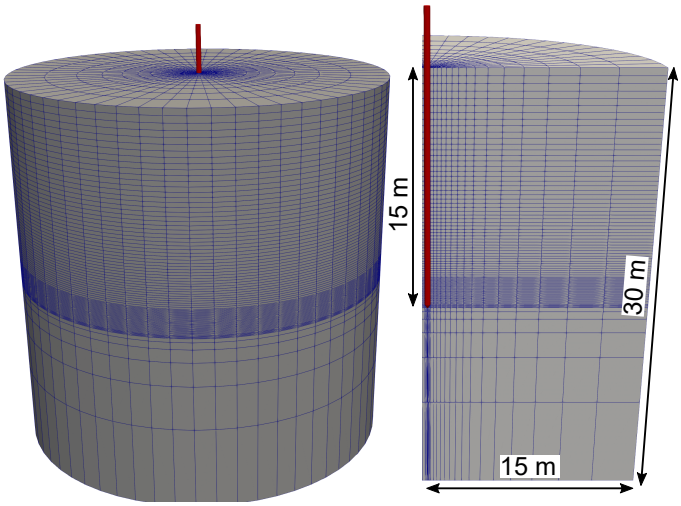

Fig. 5: Fully Lagrangian finite element model for the simulations with the HCA model

be met. In order to perform hydro-mechanically coupled analyses, a **u**-**U** finite element formulation is chosen, for which the displacement of the solid phase **u** and the displacement of the water phase **U** are spatially discretised. The basics of this formulation can be found in [55] and details on the implementation in `numgeo` in [21, 36]. For these elements, the pore water pressure is an integration point variable and calculated based on the volumetric strain of the two phases. Only the ground surface allows for drainage by not prescribing the water displacement normal to the boundary. At the soil vibrator interface, the water displacement normal to the vibrator is coupled with the displacement of the solid by means of a penalty approach, such that the water can not penetrate into the vibrator. Therefore, no drainage is possible via the vibrator-soil interface.

The finite-element model is shown in Fig. 5. It has a total of approximately 100,000 nodes, with 6 degrees of freedom per node. The direct solver `MUMPS` (MUltifrontal Massively Parallel sparse direct Solver) [1, 2] is used to solve the system of equations.

A zero-thickness element-based mortar contact discretisation scheme with four integration points per element face is used for the soil-pile interface. Details on the contact discretisation method and its implementation can be found in [44, 43]. A simple Coulomb friction model with a friction coefficient of $\mu = 0.3$ is adopted.

Only the high-cycle phase of HCA model is performed in the Lagrangian analysis, since the strain amplitude has already been determined in the CEL calculations, i.e. the low-cycle phase indicated in Fig. 3 is not required for the analyses using the Lagrangian model. In order to simulate multiple stages of vibro compaction, the following steps are undertaken:

1. Obtain the state variables and the strain amplitude in the initial depth of the vibrator by means of dynamic CEL analyses. This procedure is identical to the one explained in Section 3.

2. Simulate N cycles (or time $t = N/f$, where f is the frequency) of the vibrator using the HCA model with the calculated strain amplitude as input. This results in a change of state variables (void ratio, total stress, pore water pressure and the cyclic history state variable g^A of the HCA model) in the entire model. A transient analysis is performed, considering excess pore water pressures and consolidation. As mentioned earlier, a frequency of vibration of 25 Hz is considered, which influences inertia effects and the consolidation process. Different vibration times Δt per compaction stage are considered, as is explained later.

3. Pulling of the vibrator by Δz by spatially shifting the strain amplitude by Δz during the analysis. At the same time, the reference stiffness E^0 used in Eq. (2) is shifted likewise. The strain amplitude at the new spatial position is then scaled by Eq. (2) using the current

stiffness E^N (influenced by the compaction phases performed earlier) at this spatial position. Following the scaling, the spatial distribution of the strain amplitude is spatially smoothed using Eq. (3). All other state variables of the soil (void ratio, effective stresses, cyclic history) remain unaltered by this procedure. The feasibility of scaling the strain amplitude using the change in stiffness has been demonstrated in [40] and has been validated based on undrained cyclic triaxial tests, amongst others.

4. Simulate N cycles using the spatially updated field of strain amplitude.

5. Repeat from step 3 until the final compaction stage, viz. $\sum_i \Delta z_i = z_{\text{final}}$

With this procedure it is possible to consider a large number of compaction stages i with a nearly arbitrary large number of cycles N per stage in one simulation. The scaling of the strain amplitude is possible, since the displacement amplitude of the vibrator is assumed to be constant for each stage. Otherwise, such an approach would not be feasible. Note that the vibrator itself is not shifted, i.e. it is fixed to its initial position. Therefore, the loosening of the soil occurring when the cavity forming below the vibrator tip following the pulling is filled again by soil is not taken into account. Only shifts directed to the ground surface are considered.

Figure 6 shows the results of the simulation of the DVC process considering 15 stages of compaction with a duration of 60 s (1,500 cycles) per stage. The hydraulic conductivity of the soil is $k^w = 10^{-3}$ m/s. The vibrator is pulled in steps of $\Delta z = 1$ m, such that starting in a depth of 15 m, the tip of the vibrator is 1 m below the ground surface in the last compaction phase. The upper part of the figure displays the spatial distribution of the strain amplitude at compaction stages of 0 m, 2 m, 4 m, 6 m and 10 m. The initial distribution of the strain amplitude at $\Delta z = 0$ m is identical to the one obtained from the CEL simulations. As explained earlier, at each compaction stage, the spatial distribution of the strain amplitude is first shifted by Δz with respect to the reference position and then scaled by the current stiffness of the soil considering the shifted reference value. With increasing Δz the zone of large values of strain amplitude increases, which is due to the lower stiffness of the soil with decreasing overburden height. In addition, since excess pore water pressures develop during the compaction which are not fully dissipated at the time the vibrator is pulled, the stiffness of the soil is further reduced. The spatial distribution of relative density at the end of each phase demonstrates the effectiveness of the DVC process, leading to a compaction of the soil in a large zone around the vibrator. A cone-shaped distribution is obtained after 10 compaction phases, with an average radius from the vibrator of approximately 4-5 m. Unsurprisingly, stronger compaction occurs in a distance of 1-2 m to the vibrator compared to greater distances. In line with observations from practice, loosening of the soil close to the ground surface occurs, necessitating the implementation of additional soil compaction procedures. In case of the pore water pressure, the shown distribution is at the maximum value of excess pore water pressure for each compaction stage, which is approximately at 50-75 cycles of the vibrator. It is well visible that the excess pore water pressure generated by the DVC process decreases with increasing number of compaction stages which is due to the densification of the soil caused by the compaction stages performed prior. However, despite the comparably high hydraulic conductivity of $k^w = 10^{-3}$ m/s, considerable excess pore water pressures are observed for the first three compaction phases.

The excess pore water pressure and relative density with respect to the depth below the ground surface in a distance of 1 m to the vibrator are shown in Fig. 7. The distributions at different distances of the vibrator to its original position are given. As in case of Fig. 6, the shown distribution of excess pore water pressure is obtained at the time with maximum value of excess pore water pressure for each compaction stage. In case of the relative density the values at the end of each phase are given. At the initial stage (0 m), the vibration causes positive excess pore water pressures at the tip of the vibrator (15 m), but negative excess pore water pressures for depths both lower than 11 m or higher than 18 m. In contrast, during the second phase of compaction (tip of vibrator is located 13 m below the ground surface), only positive excess pore water pressures develop, with the peak value being located at approximately 13 m. Slightly lower excess pore water pressures are observed after pulling the vibrator by $\sum_i^4 \Delta z_i = 4$ m, which is due to the compaction the soil has already experienced in the first three stages of vibration.

The distribution of the relative density at $\Delta z =$

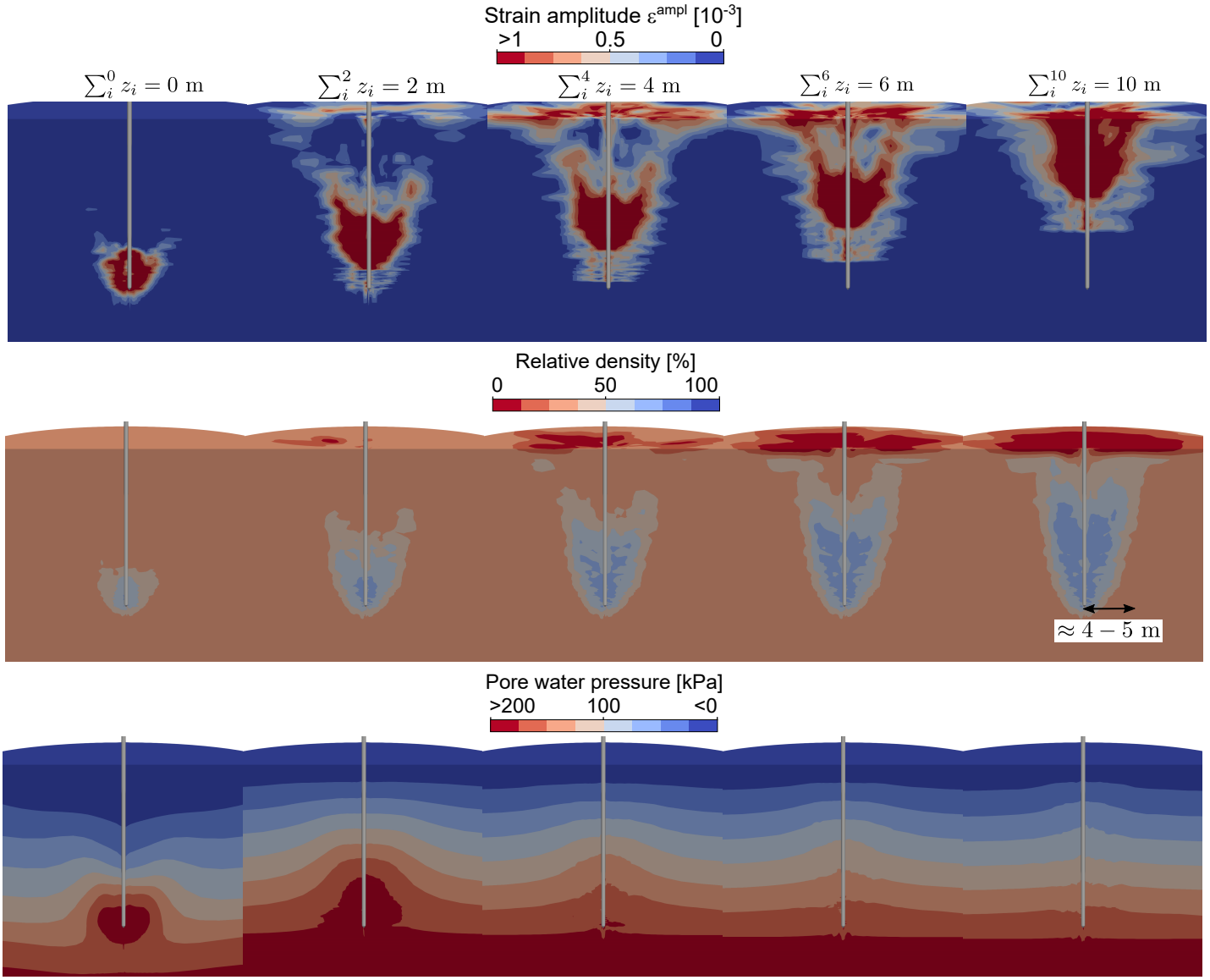

Fig. 6: Field of the strain amplitude, the relative density and the pore water pressure for each stage of the DVC process pulling the vibrator in steps of $\Delta z = 1$ m with a duration of 60 s per compaction stage

0 m shows that the vibration causes densification in a zone identical to the zone of positive excess pore water pressure. A slight loosening is observed in zones closer to the ground surface which experience negative excess pore water pressure. Relative densities of 60 % are reached at the height of the tip of the vibrator at the end of the first stage. This value increases further with increasing number of compaction phases, which can be seen from the distribution at 4 m. The distributions at 8 m, 10 m and 14 m demonstrate that the location of maximum compaction is always in greater depths below the ground surface than the location of the tip of the vibrator at the current compaction stage. Although the vibrator is 1 m below the soil surface in the last phase, values of relative density of less than 60 % are achieved in the upper 3-4 m. In addition, the last vibration phase also results in a strong loosening of the soil at the ground surface, resulting in the loosest possible state of the soil. In fact, close to the ground surface, the relative density decreases further with each compaction stage. These results clearly demonstrate the necessity of additional near-surface compaction following the DVC process [17].

An important question in practice is the estimation of the distance Δz between compaction stages and the vibration time per stage Δt. Figure 8 compares the vertical distribution of relative density in a horizontal distance of 1 m to the vibrator for two different configurations: The vibrator is either pulled in steps of $\Delta z = 0.5$ m with a duration of

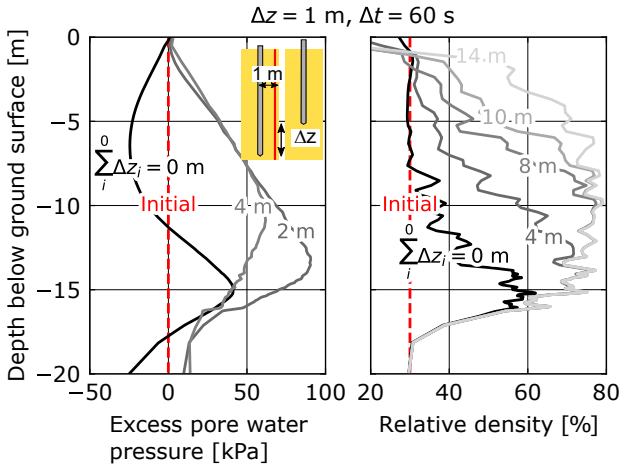

Fig. 7: Excess pore water pressure and relative density vs. depth below the ground surface in a distance of 1 m to the vibrator pulling the vibrator in steps of $\Delta z = 1$ m with a duration of 60 s per compaction stage

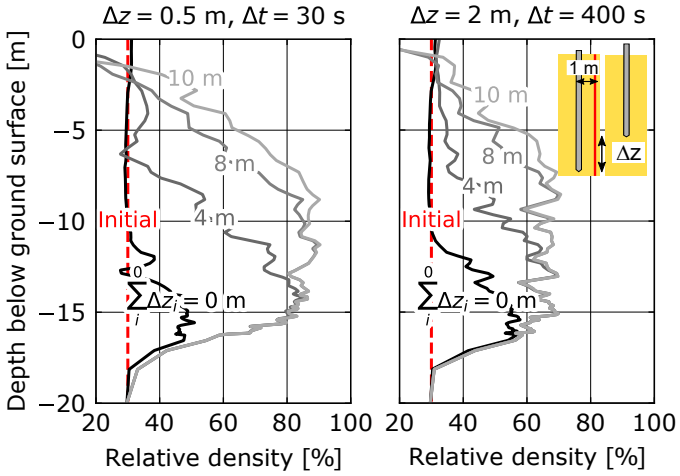

Fig. 8: Relative density vs. depth below the ground surface in a horizontal distance of 1 m to the vibrator. The vibrator is either pulled in steps of $\Delta z = 0.5$ m with a duration of 30 s per compaction stage or in steps of $\Delta z = 2$ m with a duration of 400 s per compaction stage

30 s per compaction stage or in steps of $\Delta z = 2$ m with a duration of 400 s per compaction stage. Compared to the simulation considering $\Delta t = 60$ s (Fig. 7), setting $\Delta t = 30$ s and $\Delta z = 0.5$ m results in considerably greater compaction of the soil at $\sum_i \Delta z_i = 10$ m, despite the identical total time ($11 \cdot 60$ s $= 22 \cdot 30$ s $= 660$ s, equivalent to 16,500 cycles) of vibration. Setting $\Delta z = 2$ m and $\Delta t = 400$ s the total time is greater ($5 \cdot 400$ s $= 2000$ s, equivalent to 50,000 cycles), but the DVC process leads to lower compaction compared to the other two configurations. This holds true for both the maximum values of relative density achieved and the zone of soil compacted.

To evaluate which is the optimal time of vibration per stage, Fig. 9 compares simulations with $\Delta t = \{30,\ 45,\ 75,\ 90\}$ s and $\Delta z = 1$ m. As expected, the longer the duration, the higher the compaction achieved. However, despite the much shorter total time of vibration, setting $\Delta t = 30$ s already results in considerable densification, with values of approximately 70 % for depths between 8 and 14 m. Considering a longer vibration time results in a slight increase to $D_r = 70 - 80$ % at these depths and also a slightly larger zone of compaction. Therefore, in line with the observation made based on Fig. 8 that compaction with low values of Δz and Δt should be favoured, a short period of vibration is found to be more economic. This is despite the excess pore water pressures generated by the vibration process as was demonstrated in Fig. 7.

DVC is only an appropriated ground improvement technique for medium fine to coarse sands with no or low fines content. To demonstrate how the hydraulic conductivity of the soil influences the compaction process, the results of a simulation setting $k^w = 10^{-4}$ m/s, $\Delta z = 1$ m and $\Delta t = 90$ s are shown in Fig. 10. In analogy to Fig. 7 the distribution of excess pore water pressure is shown for the maximum value during the compaction stage (again, approximately at 75 cycles of the vibrator after the start in each stage). Unsurprisingly, the lower value of k^w results in higher excess pore water pressures compared to $k^w = 10^{-3}$ m/s given in Fig. 7. The peak value of excess pore water pressure is observed to be shifted downwards relative to the location of the tip of the vibrator, which is due to the remaining excess pore water pressure from the earlier stages. Compared to the right-hand side of Fig. 9, the simulation assuming $k^w = 10^{-4}$ m/s shows a much lower compaction of the soil, in particular for lower depths below the ground surface. Overall, the simulations show that DVC is not efficient in increasing the relative density of the soil for $k^w = 10^{-4}$ m/s.

5 Conclusions & Outlook

A numerical approach to calculate the changes in the state of loose granular soils caused by deep vibro compaction (DVC) has been presented. The scheme utilises a high-cycle accumulation model for sand together with an adaptive definition of

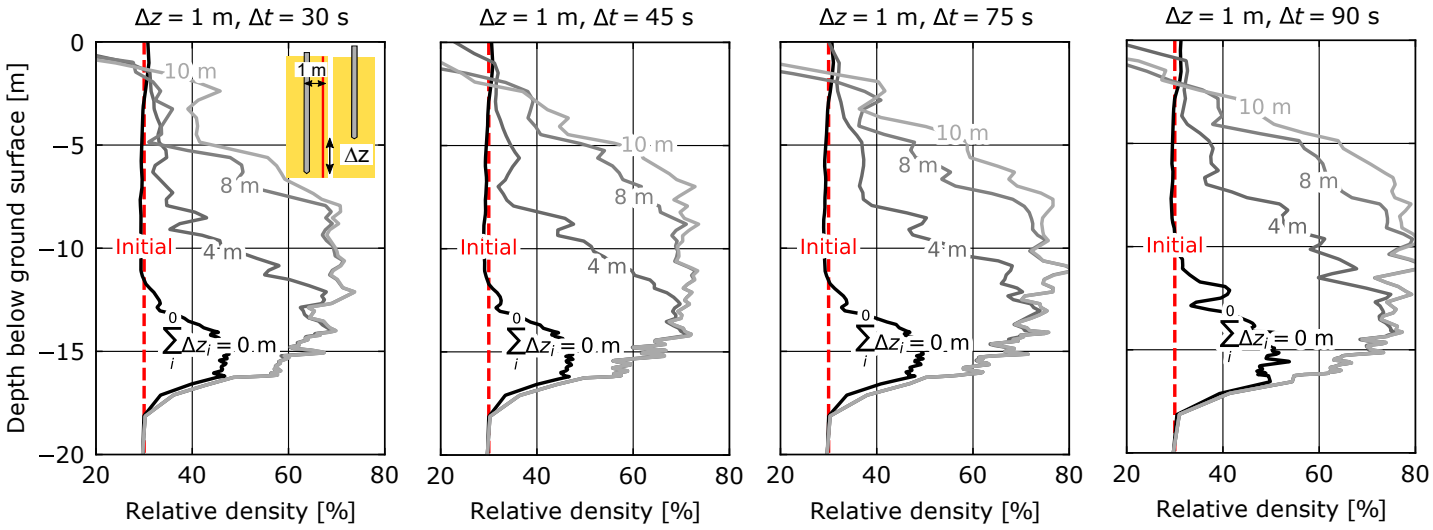

Fig. 9: Relative density vs. depth below the ground surface in a horizontal distance of 1 m to the vibrator pulling the vibrator in steps of $\Delta z = 1$ m with a duration of $\Delta t = \{30, 45, 75, 90\}$ s per compaction stage

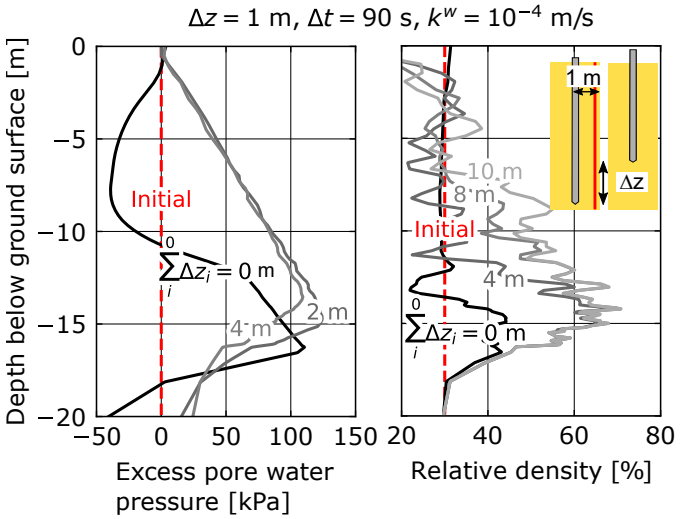

Fig. 10: Excess pore water pressure and relative density vs. depth below the ground surface in a horizontal distance of 1 m to the vibrator pulling the vibrator in steps of $\Delta z = 1$ m with a duration of 90 s per compaction stage

the strain amplitude. In contrast to existing approaches, the developed scheme allows to realistically consider an arbitrary large number of cycles exerted by the vibrator and multiples stages of compaction. The following conclusions were drawn from the analyses performed:

- The vertical distance between compaction stages and the duration of vibration per stage influence the change in relative density considerably, even if the total time of the complete process is identical.
- Longer vibration times of 400 s and larger distances between compaction stages of 2 m result in lower final relative densities as shorter (60 s or 30 s) but more frequent stages (distance of 1 m or 0.5 m), despite a longer total time of vibration. Therefore, shorter and more frequent compaction stages are found to be more efficient, which is in line with experience from practice.
- Even for a value of hydraulic conductivity of $k^w = 10^{-3}$ m/s the DVC process lead to considerable excess pore water pressures. For soils with values of hydraulic conductivity lower than $k^w = 10^{-4}$ m/s, simulations indicate that the method is not suitable to achieve a satisfactory compaction.

Because of the high effective stresses developing during the DVC process, particle breakage may occur. Future research will incorporate the model proposed in [10] to account for such effects. Furthermore, the numerical scheme proposed in this work will be validated by field or model tests [26] in a follow-up work.

Data availability statement

Some or all data, models, or code that support the findings of this study are available from the corresponding author upon reasonable request. `numgeo` can be freely downloaded from `www.numgeo.de`. The input files used can be obtained from the corresponding author or may be directly downloaded from `www.numgeo.de`.

Acknowledgements

Parts of this research were funded by German Research Council (DFG) in the framework of the project No. TR 218/28-1. The financial support by DFG is gratefully acknowledged herewith.

References

[1] P. R. Amestoy, I. S. Duff, J.-Y. L'Excellent, and J. Koster. "A Fully Asynchronous Multifrontal Solver Using Distributed Dynamic Scheduling". In: {*SIAM*} *Journal on Matrix Analysis and Applications* 23.1 (2001), pp. 15–41. ISSN: 0895-4798. DOI: 10.1137/s0895479899358194.

[2] P. R. Amestoy, A. Guermouche, J.-Y. L'Excellent, and S. Pralet. "Hybrid scheduling for the parallel solution of linear systems". In: *Parallel Computing* 32.2 (2006), pp. 136–156. ISSN: 0167-8191. DOI: 10.1016/j.parco.2005.07.004.

[3] M. Arnold and I. Herle. "Comparison of vibrocompaction methods by numerical simulations". In: *International Journal for Numerical and Analytical Methods in Geomechanics* 33.16 (2009), pp. 1823–1838. ISSN: 03639061. DOI: 10.1002/nag.798.

[4] A. Bolton. *Future of airports: Making space for Singapore's Changi airport expansion.* Zugriff am 15.11.2020.

[5] W. Fellin, G. Hochenwarter, and A. Geiss. "On-line Verdichtungskontrolle bei der Rütteldruckverdichtung". In: *Messen in der Geotechnik 2002: Mitteilungen des Institutes für Grundbau und Bodenmechanik, Technische Universität Braunschweig* 68 (2015), pp. 87–106.

[6] T. Hamann, G. Qiu, and J. Grabe. "Application of a Coupled Eulerian-Lagrangian approach on pile installation problems under partially drained conditions". In: *Computers and Geotechnics* 63 (2015), pp. 279–290. ISSN: 0266-352X. DOI: https://doi.org/10.1016/j.compgeo.2014.10.006.

[7] E. Heins and J. Grabe. "Class-A-prediction of lateral pile deformation with respect to vibratory and impact pile driving". In: *Computers and Geotechnics* 86 (2017), pp. 108–119. ISSN: 18737633. DOI: 10.1016/j.compgeo.2017.01.007.

[8] E. Heins, K.-F. Seitz, A. Chmelnizkij, M. Milatz, and J. Grabe. "Advances in Numerical Modelling of Different Ground Improvement Techniques". In: *Geotechnical Engineering Journal of the SEAGS & AGSSEA* 48.98 (2017).

[9] T. J. Hughes and J. Winget. "Finite rotation effects in numerical integration of rate constitutive equations arising in large deformation analysis". In: *International Journal for Numerical Methods in Engineering* 15.12 (1980), pp. 1862–1867. ISSN: 10970207. DOI: 10.1002/nme.1620151210.

[10] N. Irani, A. Lashkari, M. Tafili, and T. Wichtmann. "A state-dependent hyperelastic-plastic constitutive model considering shear-induced particle breakage in granular soils". In: *Acta Geotechnica* 17.11 (2022), pp. 5275–5298. ISSN: 1861-1133. DOI: 10.1007/s11440-022-01636-z.

[11] G. Jaumann. "Geschlossenes System physikalischer und chemischer Differentialgesetze". In: *Sitzber. Akad. Wiss. Wien (IIa)* 120 (1911), pp. 385–530.

[12] H. P. Jostad, B. M. Dahl, A. Page, N. Sivasithamparam, and H. Sturm. "Evaluation of soil models for improved design of offshore wind turbine foundations in dense sand". In: *Geotechnique* 70.8 (2020), pp. 682–699. ISSN: 17517656. DOI: 10.1680/jgeot.19.TI.034.

[13] Keller Holding GmbH. *Hauptprospekt 10-02D: Die Tiefenrüttelverfahren.* Keller Publications 2015 (DVD). 2015.

[14] S. Keßler, G. Heibrock, and T. Triantafyllidis. "On prediction of vibrocompaction performance using numerical models". In: *TRANSVIB 2006: Symposium International sur le Vibrofonçage et la Vibrocompaction.* Ed. by H. Gonin and A. Holeyman. Paris: LCPC, 2006, pp. 233–242.

[15] I. Kimmig, T. Triantafyllidis, and L. Knittel. "Experimentelle, analytische und numerische Untersuchungen zur Verdichtungsprognose von Sand bei der Rütteldruckverdichtung". In: *Bautechnik* 96.10 (2019), pp. 760–772. DOI: 10.1002/bate.201900038.

[16] I. Kimmig. "Untersuchungen zur Verdichtungsprognose von Sand bei der Rütteldruckverdichtung". PhD thesis. Publications of the Institute of Soil Mechanics and Rock Mechanics, Karlsruhe Institute of Technology, Issue No. 190, 2021, p. 218.

[17] K. Kirsch and F. Kirsch. *Ground Improvement by Deep Vibratory Methods*. Second Edition. Boca Raton: Taylor & Francis, CRC Press, 2017.

[18] L. Krogh, S. Quinteros, H. K. Engin, and T. Lunne. "Revisiting interpretation of relative density from shallow depth CPTs in sand". In: *Canadian Geotechnical Journal* 59.6 (Aug. 2021), pp. 808–826. ISSN: 0008-3674. DOI: 10.1139/cgj-2021-0200.

[19] J. Machaček, T. Wichtmann, H. Zachert, and T. Triantafyllidis. "Long-term settlements of a ship lock: measurements vs. FE-prediction using a high cycle accumulation model". In: *Computers and Geotechnics* 97.5 (2018), pp. 222–232.

[20] J. Machaček, P. Staubach, M. Tafili, H. Zachert, and T. Wichtmann. "Investigation of three sophisticated constitutive soil models: From numerical formulations to element tests and the analysis of vibratory pile driving tests". In: *Computers and Geotechnics* 138 (2021), p. 104276. ISSN: 18737633. DOI: 10.1016/j.compgeo.2021.104276.

[21] J. Machaček, T. Triantafyllidis, and P. Staubach. "Fully coupled simulation of an opencast mine subjected to earthquake loading". In: *Soil Dynamics and Earthquake Engineering* 115 (2018), pp. 853–867. ISSN: 02677261. DOI: 10.1016/j.soildyn.2018.09.016.

[22] J. Machaček. *Contributions to the Numerical Modelling of Saturated and Unsaturated Soils*. Dissertation, Publications of the Institute of Soil Mechanics and Rock Mechanics, Karlsruhe Institute of Technology, Issue No. 187. 2020.

[23] K. R. Massarsch and B. H. Fellenius. "Chapter 4 - Deep Vibratory Compaction of Granular Soils". In: *Ground Improvement Case Histories*. Ed. by B. Indraratna, J. Chu, and C. Rujikiatkamjorn. San Diego: Butterworth-Heinemann, 2015, pp. 111–135. ISBN: 978-0-08-100698-6. DOI: https://doi.org/10.1016/B978-0-08-100698-6.00004-0.

[24] S. Nagula and J. Grabe. "Coupled Eulerian Lagrangian based numerical modelling of vibro-compaction with model vibrator". In: *Computers and Geotechnics* 123 (2020), p. 103545. DOI: 10.1016/j.compgeo.2020.103545.

[25] S. Nagula, M. Nguyen, J. Grabe, J. Kardel, and T. Bahl. "Field measurements and numerical analysis of vibroflotation of sand". In: *Géotechnique* 72.10 (2022), pp. 882–898. DOI: 10.1680/jgeot.20.p.195.

[26] S. S. Nagula and J. Grabe. "Coupled Eulerian Lagrangian based numerical modelling of vibro-compaction with model vibrator". In: *Computers and Geotechnics* 123 (2020), p. 103545. ISSN: 18737633. DOI: 10.1016/j.compgeo.2020.103545.

[27] S. S. Nagula, Y. W. Hwang, S. Dashti, and J. Grabe. "Numerical investigation of liquefaction mitigation potential with vibroflotation". In: *Soil Dynamics and Earthquake Engineering* 146 (2021), p. 106736. ISSN: 02677261. DOI: 10.1016/j.soildyn.2021.106736.

[28] P. Nagy. "Rütteldruckverdichtung: dynamische Verdichtungskontrolle auf Basis der Rüttlerbewegung". PhD thesis. Technische Universität Wien, 2018.

[29] P. Nagy, D. Adam, F. Kopf, and P. Freitag. "Experimental and theoretical investigation of deep vibro compaction". In: *XVI Danube - European Conference on Geotechnical Engineering*. Paper No. 087. Skopje, Macedonia, June 2018. DOI: 10.1002/cepa.756.

[30] P. Nagy, D. Adam, F. Kopf, P. Freitag, W. Smon, and C. Kummerer. *Dokumentation der Messdaten in Punkt 51 am Changi Airport Singapore*. internal, not published. Nov. 2019.

[31] A. Niemunis, T. Wichtmann, and T. Triantafyllidis. "A high-cycle accumulation model for sand". In: *Computers and Geotechnics* 32.4 (2005), pp. 245–263. DOI: https://doi.org/10.1016/j.compgeo.2005.03.002.

[32] A. Niemunis and I. Herle. "Hypoplastic model for cohesionless soils with elastic strain range". In: *Mechanics of Cohesive-Frictional Materials* 2.4 (1997), pp. 279–299. ISSN: 10825010. DOI: 10.1002/(SICI)1099-1484(199710)2:4<279::AID-CFM29>3.0.CO;2-8.

[33] A. Niemunis, T. Wichtmann, and T. Triantafyllidis. "A high-cycle accumulation model for sand". In: *Computers and Geotechnics* 32.4 (2005), pp. 245–263. ISSN: 0266352X. DOI: 10.1016/j.compgeo.2005.03.002.

[34] A. M. Page, R. T. Klinkvort, S. Bayton, Y. Zhang, and H. P. Jostad. "A procedure for predicting the permanent rotation of monopiles in sand supporting offshore wind turbines". In: *Marine Structures* 75 (Jan. 2021), p. 102813. ISSN: 09518339. DOI: 10.1016/j.marstruc.2020.102813.

[35] V. R. Raju and W. Sondermann. "Chapter 6 - Ground Improvement Using Deep Vibro Techniques". In: *Ground Improvement Case Histories*. Ed. by B. Indraratna, J. Chu, and C. Rujikiatkamjorn. San Diego: Butterworth-Heinemann, 2015, pp. 175–213. ISBN: 978-0-08-100698-6. DOI: https://doi.org/10.1016/B978-0-08-100698-6.00006-4.

[36] P. Staubach and J. Machaček. "Influence of relative acceleration in saturated sand: Analytical approach and simulation of vibratory pile driving tests". In: *Computers and Geotechnics* 112 (Aug. 2019), pp. 173–184. ISSN: 0266352X. DOI: 10.1016/j.compgeo.2019.03.027.

[37] P. Staubach, J. Machaček, R. Sharif, and T. Wichtmann. "Back-analysis of model tests on piles in sand subjected to long-term lateral cyclic loading: Impact of the pile installation and application of the HCA model". In: *Computers and Geotechnics* 134 (June 2021), p. 104018. ISSN: 0266352X. DOI: 10.1016/j.compgeo.2021.104018.

[38] P. Staubach. "Contributions to the numerical modelling of pile installation processes and high-cyclic loading of soils". PhD Thesis. Publications of the Chair of Soil Mechanics, Foundation Engineering and Environmental Geotechnics, Ruhr-University Bochum, Issue No. 73, 2022.

[39] P. Staubach, J. Machaček, M. C. Moscoso, and T. Wichtmann. "Impact of the installation on the long-term cyclic behaviour of piles in sand: A numerical study". In: *Soil Dynamics and Earthquake Engineering* 138 (2020), p. 106223. ISSN: 02677261. DOI: 10.1016/j.soildyn.2020.106223.

[40] P. Staubach, J. Machaček, L. Tschirschky, and T. Wichtmann. "Enhancement of a high-cycle accumulation model by an adaptive strain amplitude and its application to monopile foundations". In: *International Journal for Numerical and Analytical Methods in Geomechanics* 46.2 (Feb. 2022), pp. 315–338. ISSN: 0363-9061. DOI: 10.1002/nag.3301.

[41] P. Staubach and T. Wichtmann. "Long-term deformations of monopile foundations for offshore wind turbines studied with a high-cycle accumulation model". In: *Computers and Geotechnics* 124 (Aug. 2020), p. 103553. ISSN: 0266352X. DOI: 10.1016/j.compgeo.2020.103553.

[42] P. Staubach, J. Machaček, M. Tafili, and T. Wichtmann. "A high-cycle accumulation model for clay and its application to monopile foundations". In: *Acta Geotechnica* 17.3 (Mar. 2022), pp. 677–698. ISSN: 1861-1125. DOI: 10.1007/s11440-021-01446-9.

[43] P. Staubach, J. Machaček, and T. Wichtmann. "Mortar contact discretisation methods incorporating interface models based on Hypoplasticity and Sanisand: Application to vibratory pile driving". In: *Computers and Geotechnics* 146 (June 2022), p. 104677. ISSN: 0266352X. DOI: 10.1016/j.compgeo.2022.104677.

[44] P. Staubach, J. Machaček, and T. Wichtmann. "Novel approach to apply existing constitutive soil models to the modelling of interfaces". In: *International Journal for Numerical and Analytical Methods in Geomechanics* 46.7 (May 2022), pp. 1241–1271. ISSN: 0363-9061. DOI: 10.1002/nag.3344.

[45] T. Triantafyllidis and I. Kimmig. "A simplified model for vibro compaction of granular soils". In: *Soil Dynamics and Earthquake Engineering* 122 (2019), pp. 261–273. DOI: 10.1016/j.soildyn.2014.12.011.

[46] T. Wichtmann. *Explicit accumulation model for non-cohesive soils under cyclic loading*. PhD thesis, Publications of the Institute of Foundation Engineering and Soil Mechanics, Ruhr-University Bochum, Issue No. 38. 2005.

[47] T. Wichtmann. *Soil Behaviour Under Cyclic Loading: Experimental Observations, Constitutive Description and Applications*. Habilitation, Institute of Soil Mechanics and Rock Mechanics, Karlsruhe Institute of Technology, Issue No. 181, 2016.

[48] T. Wichtmann, J. Machaček, H. Zachert, and H. Günther. "Validierung eines hochzyklischen Akkumulationsmodells anhand von Modellversuchen und Messungen an realen Bauwerken". In: *Bautechnik* 96.2 (2018).

[49] T. Wichtmann, A. Niemunis, and T. Triantafyllidis. "Experimental evidence of a unique flow rule of non-cohesive soils under high-cyclic loading". In: *Acta Geotechnica* 1.1 (2006), pp. 59–73.

[50] T. Wichtmann, A. Niemunis, and T. Triantafyllidis. "Improved simplified calibration procedure for a high-cycle accumulation model". In: *Soil Dynamics and Earthquake Engineering* 70.3 (2015), pp. 118–132. ISSN: 02677261. DOI: 10.1016/j.soildyn.2014.12.011.

[51] P.-A. von Wolffersdorff. "A hypoplastic relation for granular materials with a predefined limit state surface". In: *Mechanics of Cohesive-Frictional Materials* 1 (1996), pp. 251–271.

[52] M. Wotzlaw, D. Aubram, and F. Rackwitz. "Untersuchung der Fluidisierungszone bei der Rütteldruckverdichtung". In: *DGGT e.V. - Fachsektionstage Geotechnik - 2. Bodenmechanik-Tagung*. Würzburg, Oct. 2019.

[53] H. Zachert, T. Wichtmann, P. Kudella, T. Triantafyllidis, and U. Hartwig. "Inspection of a high-cycle accumulation model for sand based on recalculations of a full-scale test on a gravity base foundation for offshore wind turbines". In: *Computers and Geotechnics* 126.10 (2020), p. 103727.

[54] S. Zaremba. "Sur une forme perfectionée de la théorie de la relaxation". In: *Bull. Int. Acad. Sci. Cracovie* (1903), pp. 594–614.

[55] O. C. Zienkiewicz and T. Shiomi. "Dynamic behaviour of saturated porous media: The generalized Biot formulation and its numerical solution". In: *International Journal for Numerical and Analytical Methods in Geomechanics* 8.1 (1984), pp. 71–96. ISSN: 1096-9853. DOI: 10.1002/nag.1610080106.